Emission-Tunable CuInS$_2$/ZnS Quantum Dots: Structure, Optical Properties, and Application in White Light-Emitting Diodes with High Color Rendering Index

Po-Hsiang Chuang,[†] Chun Che Lin,[†] and Ru-Shi Liu*,[†,‡]

[†]Department of Chemistry, National Taiwan University, Taipei 106, Taiwan

[‡]Department of Mechanical Engineering and Graduate Institute of Manufacturing Technology, National Taipei University of Technology, Taipei 106, Taiwan

ABSTRACT: Synthesis and application of CuInS$_2$/ZnS core/shell quantum dots (QDs) with varying [Cu]/[In] ratios were conducted using a stepwise solvothermal route. CuInS$_2$ (CIS) core QDs with varying [Cu]/[In] ratios exhibited deep-red emissions result from donor−acceptor pair recombination. The absorption and emission band gap of the CuInS$_2$ QDs increased with the decrease in Cu content. The emission bands of the CuInS$_2$/ZnS were tuned from 550 to 616 nm by controlling the [Cu]/[In] ratio after coating ZnS layer. The CIS QDs model was developed to elucidate the synthesized crystal structure and photoluminescence of the QDs with various [Cu]/[In] ratios. Temperature-dependent photoluminescence spectra of the CIS/ZnS QDs were also investigated. The temperature dependency of the photoluminescence energy and intensity for various CIS/ZnS QDs were studied from 25 to 200 °C. Efficient white light-emitting diodes with high color rendering index values (Ra = 90) were fabricated using CIS/ZnS QDs as color converters in combination with green light-emitting Ba$_2$SiO$_4$:Eu^{2+} phosphors and blue light-emitting diodes.

KEYWORDS: CuInS$_2$, quantum dots, donor−acceptor pair, temperature-dependent photoluminescence, light-emitting diodes, color rendering index
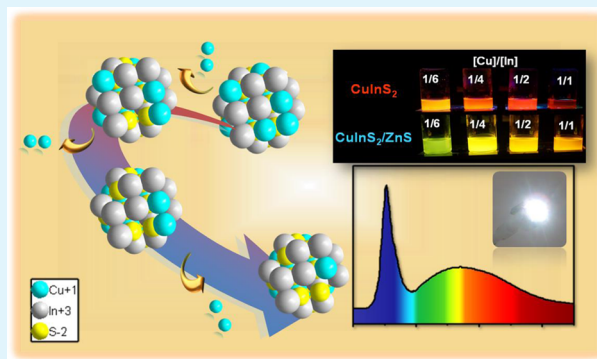
1. INTRODUCTION

Semiconductor quantum dots (QDs) have shown significant promise as light emitters, as solar cells, and in biological imaging.[1−5] Although II−VI Cd-based QDs have received much optical interest, Cd-based QDs are potentially toxic to humans and the environment. Other materials, such as binary III−V (InP) compounds[6,7] and ternary I−III−VI compounds, have been considered as replacements to conventional Cd-based QDs. The syntheses and optical properties of ternary I−III−VI compounds, including CuInS$_2$ (CIS),[8−12] CuInSe$_2$ (CISe),[13−15] CuGaS$_2$ (CGS),[16] AgInS$_2$ (AIS),[17,18] and AgGaS$_2$ (AGS),[19] have been extensively examined. Particularly, not only do CIS QDs exhibit a large absorption coefficient but also they are nontoxic. Therefore, CIS QDs have been extensively investigated. CIS QDs are generally synthesized by heating[9,20,21] and hot injection.[14,22,23] The solvothermal method may provide advantages, including facileness and mass production; QDs consequently perform various size distributions. However, various QD sizes are beneficial for different applications, such as light-emitting diodes (LEDs) for illumination and biological imaging. Especially, the major relaxation process in CIS QDs is the DAP (donor and acceptor pair) recombination, where the electron and the hole pair are recombined from donor to acceptor level within the

bandgap.[24−26] The bandgap of CIS QDs relies on the amount of [Cu]/[In], in which a wider bandgap is found in more Cu-deficient CIS QDs. Although deficient control in CIS QDs has been reported, further investigations about the effects on chemical and physical properties of CIS QDs are needed. To synthesize highly fluorescent QDs, the core/shell structures of QDs are examined. Typically, the surface of the CIS core was passivated by ZnS shell inorganic material to improve the fluorescence of QDs. Song and Yang[27] reported 67% to 78% quantum yield (QY) from CIS/ZnS QDs. Chen et al.[28] also synthesized high-quality CIS/ZnS QDs at the gram scale. These previous studies show that photoluminescence (PL), QY, and tunable emission of CIS/ZnS QDs significantly depend on the synthetic process.

Light-emitting diodes (LEDs) have been attractive because the device proved to be environmentally friendly and have higher luminous efficiency. White LEDs (WLEDs) generally consist of InGaN blue chips with yellow-emitting Y$_3$Al$_5$O$_{12}$:Ce^{3+} (YAG:Ce) phosphors.[29] WLED systems with high luminous efficacy have been popular, but it is hard to
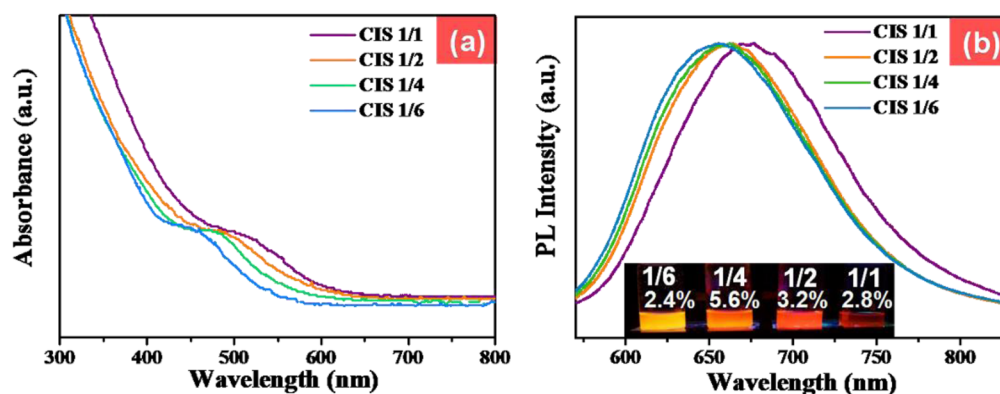
Figure 1. Optical properties of CIS QDs (a) absorption and (b) normalized PL emission spectra of CIS QDs with various [Cu]/[In] molar ratios. Inset shows the QYs and illuminations of CIS QDs under 365 nm UV lamp.
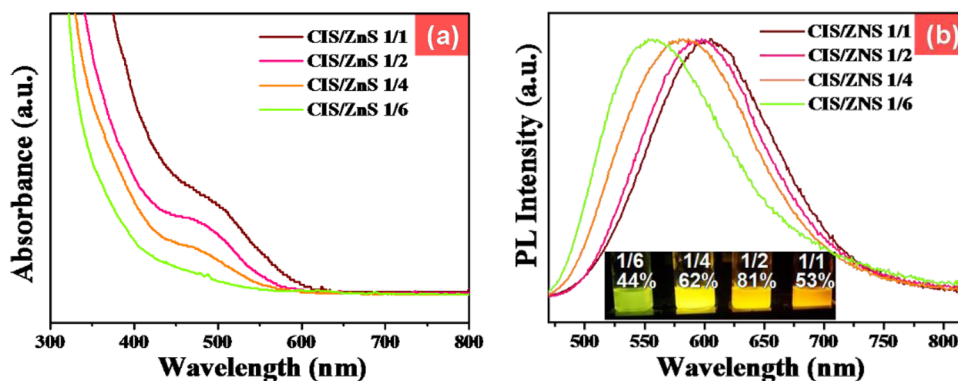

Figure 2. Optical properties of CIS/ZnS QDs (a) absorption and (b) normalized PL emission spectra of CIS/ZnS QDs with various [Cu]/[In] molar ratios. Inset shows the QYs and illuminations of CIS/ZnS QDs under 365 nm UV lamp.

acquire a high value of the color rendering index (Ra) because of the lack of the green and red spectral regions. In addition, these phosphor-converted (pc) WLEDs have low device luminous efficacy because micron-sized phosphor induces a scattering effect to lose conversion efficiency from blue to yellow light.[30,31] However, QDs have sufficiently small sizes to avoid light scattering. Therefore, several WLEDs with QDs have been developed. High-efficiency WLEDs with high Ra of 90.1 were investigated by using phosphor $Sr_3SiO_5:Ce^{3+}/Li^+$ and red-emitting CdSe QDs.[31] Ziegler et al.[32] fabricated WLEDs with a Ra index of 86, which is composed of red InP/ZnS QDs with green $Sr_{0.94}Al_2O_4:Eu_{0.06}$ and yellow YAG:Ce phosphors.

In the present study, we synthesized CIS QDs with four kinds of [Cu]/[In] molar ratios through a facile solvothermal route. The effects of Cu-deficiency on crystal lattice structure and optical properties of CIS QDs were determined. After coating the ZnS shell, the CIS/ZnS QDs exhibited tunable emission spectra and high efficiency. The temperature dependency of the photoluminescence energy and intensity for various CIS/ZnS QDs were studied from 25 to 200 °C. Furthermore, we applied green phosphor $Ba_2SiO_4:Eu^{2+}$, as well as orange- and red-light emitting CIS/ZnS QDs, to fabricate WLEDs that exhibited high color rendering index (CRI) values of ∼90.

2. EXPERIMENTAL SECTION

2.1. Materials. Copper(I) iodide (Aldrich, 99.99%), 1-dodecanethiol (DDT, Aldrich, 98%), 1-octadecene (ODE, Aldrich, 90%), indium acetate (In(Ac)₃, Alfa Aesar, 99.99%), and zinc stearate (J. T. Baker, 10−12% Zn basis) were utilized as purchased.

2.2. Synthesis of CuInS₂ Core and CuInS₂/ZnS Core/Shell QDs. CuInS₂ (CIS) core QDs were synthesized through the solvothermal route. CIS QDs with [Cu]/[In] compositions of 1/1, 1/2, 1/4, and 1/6 were synthesized with fixed amounts of In and purposely tuned amounts of Cu. Here, the synthetic procedure of CIS QDs with a [Cu]/[In] molar ratio of 1/4 is presented. CuI (0.25 mmol, 0.024 g) and In(Ac)₃ (1.0 mmol, 0.146 g) were added in a Teflon-lined autoclave; then added was 15 mL of 1-dodecanethiol (DDT), which acts as a solvent as well as sulfur precursor. The Teflon-lined autoclave was heated to a temperature of 180 °C for 5 h and 30 min. Afterward, the red product of CIS core QDs was synthesized. For improving the quantum yield, ZnS shell was coated onto the outside of the CIS QDs to form a core/shell structure. ZnS solution was prepared by mixing Zn stearate (8 mmol, 5.081g), 2 mL of DDT, and 8 mL of ODE. ZnS stock solution was combined with 15 mL of CIS QD solution and heated to 200 °C for 14 h through the solvothermal route. The CIS and CIS/ZnS QDs were cleaned several times by involving ethanol/chloroform solvent. The final precipitates were dispersed in chloroform.

2.3. Fabrication Process of CIS/ZnS QDs and Phosphor-Based White LEDs. Orange- (0.038 g) and red-emitting (0.057 g) CIS/ZnS QDs in chloroform (1 mL) were blended with 0.28 g of thermally curable silicone resin (OE-6630 B, Dow Corning Co.). After that, resin was heated to 70 °C for 1 h to evaporate the chloroform. Subsequently, an equal amount (0.28 g) of the hardener (OE-6630 A) and inorganic green-emitting (0.116 g) $Ba_2SiO_4:Eu^{2+}$ phosphor particles were added into gelatinous orange- and red-emitting CIS/ZnS QDs. Subsequently, the homogeneous silicone resin mixture of the green-emitting $Ba_2SiO_4:Eu^{2+}$ phosphor and the orange- and red-emissive CIS/ZnS QDs was dropped on the top of a blue LED chip (InGaN). The devices proceeded to be thermally cured to 80 °C for 2 h and then at 150 °C for 1 h in an oven.
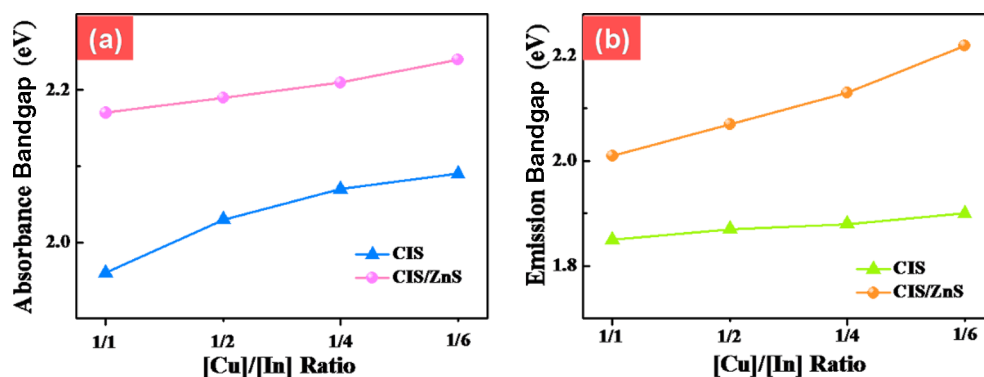
Figure 3. Variations in (a) bandgap and (b) peak emission energy of CIS/ZnS and CIS QDs with [Cu]/[In] ratios of 1/1, 1/2, 1/4, and 1/6.

2.4. Characterization. The absorption spectra of CIS and CIS/ZnS QDs were observed using UV/vis spectrophotometer (Shimadzu UV-700) and photoluminescence (PL) spectra. Thermal dependent PL spectra were measured using a FluoroMax-3 spectrophotometer with excitation at 450 nm. The structure phase of QDs was characterized by X-ray powder diffraction (XRD) using a Phaser diffractometer (Bruker D2) with Cu Kα radiation (λ = 1.5418 Å). The fluorescence quantum yields (QYs) of the CIS and CIS/ZnS QDs were measured by integrating the PL area to compare with that of rhodamine 6G (QY of 95%) in ethanol solution. Compositions of QDs were observed by X-ray photoelectron spectroscopy (XPS, Al Kα radiation, λ = 8.34 Å, PHI Quantera). Size and morphologies of QDs were characterized using transmission electron microscopy (TEM, JEOL, JEM-2100F). The luminous efficiency, electroluminescence (EL) spectrum, Commission Internationale de l'Eclairage (CIE) color coordinates, correlated color temperature, and CRI of the QD–WLEDs were evaluated, in an integrating sphere with a diode array rapid analyzer system (Everfine Photo–E-Info Co. Ltd.).

3. RESULTS AND DISCUSSION

3.1. Optical Properties of CuInS$_2$ and CuInS$_2$/ZnS QDs. CuInS$_2$ (CIS) core QDs with different [Cu]/[In] ratios were synthesized via the solvothermal method at a temperature of 180 °C for 5.5 h. The absorption spectra of CIS QDs with four kinds of ratios are shown in Figure 1a. The trend of the absorption toward longer wavelength with increasing Cu composition is observed. By tuning the [Cu]/[In] ratios in CIS QDs, the emission peak position can be tuned from 654 to 659 nm, as shown in Figure 1b. ZnS growth was added on the outside of respective CIS core QDs to form CIS/ZnS QDs. The inset of Figure 1b shows quantum yield (QY) values and illuminations of various CIS QDs under 365 nm UV lamp.

The absorption spectra of CIS/ZnS QDs with four kinds of ratios are shown in Figure 2a. The absorption position of all of the CIS/ZnS QDs shifted to a shorter wavelength compared with the corresponding original CIS QDs. This blue shift is believed to occur via cationic interdiffusion between the CIS core (bulk E_g = 1.53 eV) and the wider bandgap ZnS (bulk E_g = 3.68 eV) shell to form an alloying material on the growth surface, resulting in bandgap widening.[27] PL emissions of CIS/ZnS QDs were tuned from 558 to 618 nm with different [Cu]/[In] ratios, as shown in Figure 2b. The PL emissions of all the CIS/ZnS QDs shifted to higher energy compared with their respective original QDs. These CIS/ZnS QDs showed remarkably improved PL QYs (44–81%) with different [Cu]/[In] ratios, confirming the performance of the core/shell type. The inset of Figure 2b shows quantum yield (QY) values and illuminations of various CIS QDs under 365 nm UV lamp.

The CIS QDs are in nanoscale, so they have significantly high surface-to-volume ratios, resulting in a lot of defect sites on the surface QDs. The fluorescent features in I–III–VI QDs are entirely different from II–VI QDs or III–V QDs.[8,23,33] The full width at half-maximum (fwhm) of PL emissions for these CIS QDs are approximately 108–112 nm. Typically, I–III–VI QDs show the large difference in absorption of broad-emission band energies (Stokes shift). These results suggest that excited electron–hole pair (DAP) recombination occurred within the intraband, which is commonly defined as DAP recombination.[9,28,34] The energy levels of one acceptor (V_{Cu}: Cu vacancy) and two donors (V_S: S vacancy, In_{Cu}: Cu site was substituted in site) in bulk CIS were presented within the bandgap.[12,35] The quantized CIS QDs of electron and hole levels were widened by quantum confinement effect,[21] as well as the donor and acceptor levels moving toward conduction band (CB) and valence band (VB) levels, respectively. The dominant DAP recombination route is V_S–V_{Cu} in CIS QDs.

Radiative recombination of CIS QDs is associated with copper deficiency. The blue shift in the emission position with the increase in Cu deficiency in CIS QDs was observed because the energy gap of CIS QDs was expanded with decreasing Cu content. This phenomenon is generally attributed to the maximum VB level of CIS QDs, which is composed of hybrid orbitals of S 3p and Cu 3d,[36,37] decreasing the quantity of orbitals contributing from Cu. Therefore, Cu deficiency lowers the maximum VB level, widening the band gap of CIS QDs. [Cu]/[In] of 1/4 had the highest PL QY and was ascribed to an increase of the potentiality for DAP recombination. Notably, the optimal QYs of CIS or AgInS$_2$ QDs were synthesized with identical molar ratios of [Cu]/[In] or [Ag]/[In] of 1/4.[28,38]

However, most of these vacancies declined because of the conducting ZnS shell on the outer core. Therefore, CIS/ZnS QDs have lower V_S and V_{Cu} surface compositions. The presentation of surface donor V_S is significantly reduced, leading to minor V_S–to–V_{Cu} DAP recombination. CB–to–V_{Cu} recombination is the probable dominant transition after ZnS shell coating, resulting in a systematically blue-shifted emission.[39] This result clearly indicates that CB–to–V_{Cu} recombination may be proposed as a main route. The bandgaps (E_g) of the CIS and CIS/ZnS QDs could be estimated by the empirical formula $\alpha h\nu = (h\nu - Ex)^{1/2}$, where α is the absorption coefficient, h is Planck's constant, ν is the light frequency ($h\nu$ is the energy of a photon with frequency ν), and Ex is the optical bandgap energy.[21] The calculated absorption bandgaps of CIS and CIS/ZnS QDs with respective [Cu]/[In] ratios are plotted in Figure 3a. Compared with the CIS QDs, the bandgap of CIS/ZnS increases by 0.16 to 0.26 eV, relying

15381

dx.doi.org/10.1021/am503889z | ACS Appl. Mater. Interfaces 2014, 6, 15379–15387

on the [Cu]/[In] ratio of core QDs. This result confirms the alloying between core and shell. Moreover, the emission bandgap of CIS/ZnS compared with CIS QDs as a function of [Cu]/[In] ratio in Figure 3b shows the increase (0.14 to 0.23 eV) in the blue-shifted emission energy was larger compared to the increase (0.10 to 0.18 eV) in band gap energy.

In addition, emission in the blue shift of CIS/ZnS increased with the decrease in [Cu]/[In] molar ratios. The lower [Cu]/[In] molar ratios were utilized to generate more vacancies of Cu cations, as a result of which Zn diffuses more toward the core, which provides more vacant position to Zn cations. This evidence shows that more Cu vacancies provide more diffused Zn cations onto the CIS surface.

3.2. Crystal Structures of CIS and CIS/ZnS QDs.
Four kinds of CIS core QDs with [Cu]/[In] molar ratios were further studied through XRD to analyze their structures. The three major patterns were found, corresponding to the (112), (220)/(204), and (312)/(116) planes of the tetragonal structure. The presentation of three major patterns from the entire core QDs agrees with a chalcopyrite phase, indicating that the solvothermal method synthesizes chalcopyrite-structured CIS QDs.[8] The appearance of ZnS structure was also observed in the diffraction patterns, as shown in Figure 4. The
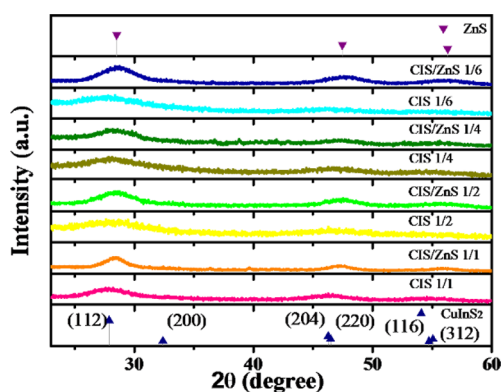

Figure 4. XRD patterns of CIS and CIS/ZnS QDs with [Cu]/[In] ratios of 1/1, 1/2, 1/4, and 1/6.

XRD patterns show that both the preformed CIS and the final CIS/ZnS QDs approve the chalcopyrite crystal structure. Notable shifts of the XRD patterns to higher 2θ values are found after deposing the ZnS shell, approaching those patterns

of the zinc-blended ZnS phase, showing that the ZnS layers were formed on the outside of CIS core QDs.[8,27,28]

The unit cell parameters of a and c in CIS QDs are evaluated using the equation $1/d^2 = (h^2 + k^2)/a^2 + l^2/c^2$, where d is the interplanar distance, h, k, and l are the Miller indices, and a and c are the unit cell parameters. Figure 5a presents the divergent a and c with different [Cu]/[In] molar ratios. The unit cell parameter "a" reduces with decreasing [Cu]/[In] ratio, whereas the parameter "c" increases. The present CIS QDs maintained the structure of chalcopyrite, even with Cu deficiency, which is consistent with the literature.[28,36] The chalcopyrite structure follows the zinc-blended structure;[40] one-half of the cations (Zn) are substituted by copper and the other half are substituted by In cations. The sulfur anions are reserved in the same site. Nevertheless, the cation position is occupied by two different kinds of atoms, resulting in a slightly distorted crystal lattice. The distances between the S^{2-} and the individual Cu^+ and In^{3+} vary in the chalcopyrite structure.[41] Therefore, tetragonal distortion can be quantified by the tetragonal distortion parameters η in I−III−VI chalcopyrite structure and can be used to determine the relationship between the a and c unit cell parameters, as $\eta = c/2a$. Figure 5b shows that the parameter η of CIS QDs changes from 0.778 to 1.027 with respective [Cu]/[In] molar ratios. The η values gradually decrease with the decrease in [Cu]/[In] ratio, indicating significant distortion of the tetragonal structure with increasing Cu deficiency. Moreover, the number of anions occupied from the original tetrahedral position is regarded as the anion displacement parameter (u), which can be evaluated as $u = 1/4 + \alpha/a^2$, where $\alpha = R_{CuS}^2 - R_{InS}^2$; R_{CuS} and R_{InS} are the respective cation−anion bond lengths.[42]

Transmission electron microscopy (TEM) analysis of the CIS QDs was observed. Figure 6a shows a CIS QD ([Cu]/[In] = 1/4) whose size was distributed in the range 2.0−2.5 nm. ZnS shell deposited on the CIS QDs ([Cu]/[In] = 1/4), and the size of core/shell QDs roughly enlarged to 3.2−4.0 nm, as shown in Figure 6b.

The surface chemical compositions of CIS and CIS/ZnS QDs were determined through X-ray photoelectron spectroscopy (XPS) characterization. The CIS core QDs with [Cu]/[In] = 1/4 showed the dominant photoelectron signals In 3d and Cu 2p, confirming that the copper and indium elements of CIS QDs are in their expected valence (Cu^+ and In^{3+}),[42,43] as shown in Figure 7a and b. With the growth of ZnS shell, the
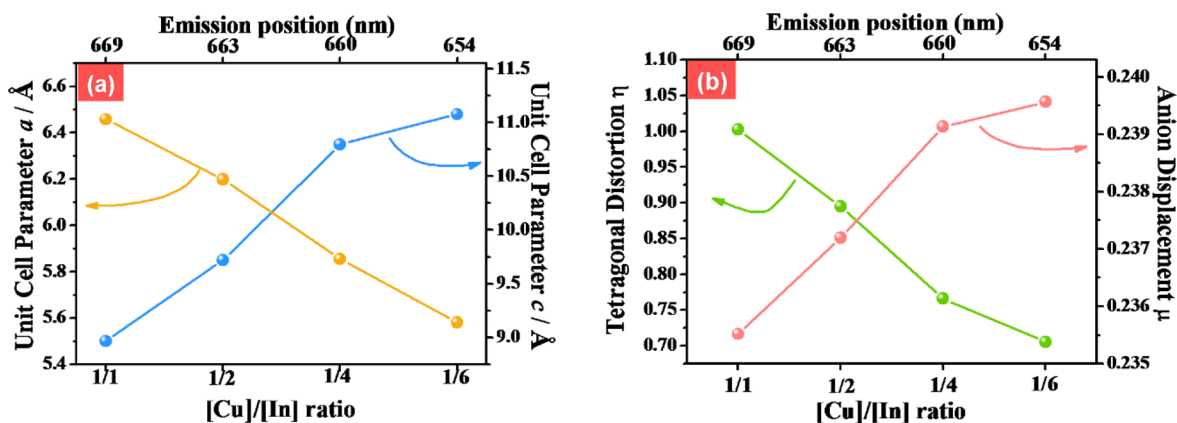

Figure 5. Plots of (a) unit cell parameters a and c and (b) tetragonal distortions and anion displacement parameters of CIS QDs as a function of their [Cu]/[In] molar ratios.
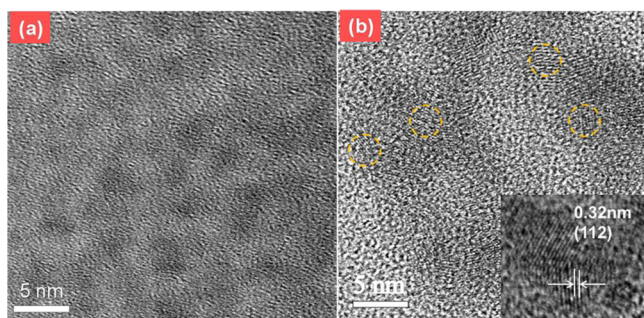
Figure 6. (a) TEM images of CIS QDs with a [Cu]/[In] ratio of 1/4. (b) TEM images of CIS/ZnS QDs with a [Cu]/[In] ratio of 1/4.

signal of Cu 2p peaks declined and the signal of In 3d peak declined in the CIS/ZnS QDs. By contrast, the Zn 2p peaks appeared due to the presence of over ZnS shell layer. This characterization qualitatively shows the elemental composition of QDs.

3.3. Thermal Stability of CIS/ZnS QDs. The ZnS layer significantly passivated the nonradiative surface of QDs and enhanced the QY.[27,28] The temperature-dependent PL spectra (TL) of CIS crystals were obtained to determine the temperature dependence of the PL spectra.[44−46] Therefore, to investigate the thermal stability of CIS/ZnS QDs, the TL of CIS/ZnS QDs with respective[Cu]/[In] molar ratios were monitored with the increase in applied temperature from 25 to 200 °C. We prepared the powdered QDs by drying in an oven. The QDs were then transferred into a holder to obtain the TL under various temperatures. The decreasing emission intensity of CIS/ZnS QDs was dependent on increasing the temper-

ature; because the nonradioactive transition from the excited states to the ground state increased, this result is defined as the thermal quenching effect. The red emission ascribed to the CIS/ZnS QDs was observed when the powder shifted to a longer wavelength than that of the powder dispersed in chloroform. Figure 8 shows the TL of CIS/ZnS QDs at 25−200 °C.

Red shift and broadening of PL bandwidth are observed with the increase in temperature. The PL intensity of CIS/ZnS QDs rapidly decreases with the increase in temperature. In general, ZnS shell significantly enhanced the PL QY, thereby eliminating nonradiative recombination sites on the surface of the QDs. The PL relaxation path for CIS/ZnS QDs is unaffected by passivation. The fwhm of the PL spectra for CIS/ZnS QDs with different [Cu]/[In] molar ratios at 25−200 °C are shown in Figure 8a.

The emission intensities of all of the CIS/ZnS QDs decrease with the increase in environmental temperature, as shown in Figure 9a. The emission intensity of the CIS/ZnS QDs of [Cu]/[In] = 1/6 decreases faster than that of the other molar ratios with the increase in temperature. This phenomenon can be attributed to the lattice structure. The present CIS/ZnS QDs maintained the chalcopyrite frame, although all of the QDs were produced with purposeful Cu deficiency. This result agreed with that in the literature.[28] The Cu-deficient QDs probably have high densities of Cu defect sites, thereby weakening the structure. Therefore, the CIS/ZnS QDs with [Cu]/[In] = 1/6 showed the lowest thermal stability.

Figure 9b shows the relative integrate area of spectra with variation of [Cu]/[In] from the temperature range 25−200 °C. The relative integrate area is associated with intensity and width of spectra. The relative integrate area for [Cu]/[In] = 1/2 is
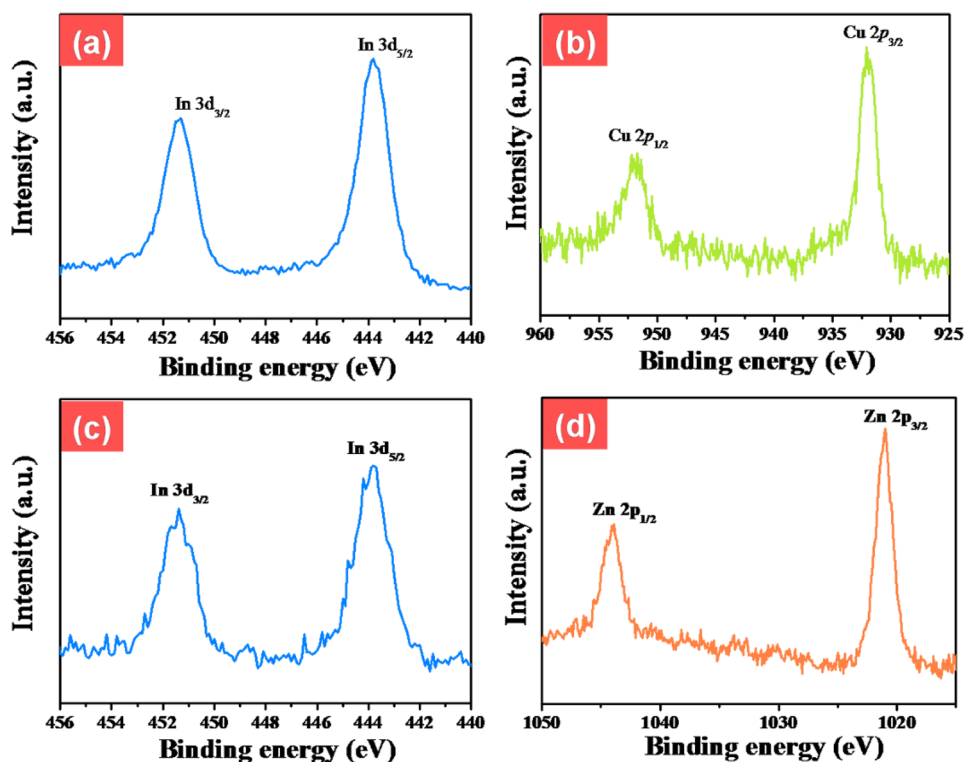

Figure 7. XPS high-resolution scans of In 3d photoelectron of (a) CIS core and (c) CIS/ZnS core/shell QDs. (b) High-resolution scan of Cu 2p photoelectron of CIS QDs. (d) High-resolution scan of Zn 2p photoelectron of CIS/ZnS core/shell QDs. CIS and CIS/ZnS QDs with Cu/In ratio of 1/4 were selected for XPS measurement.
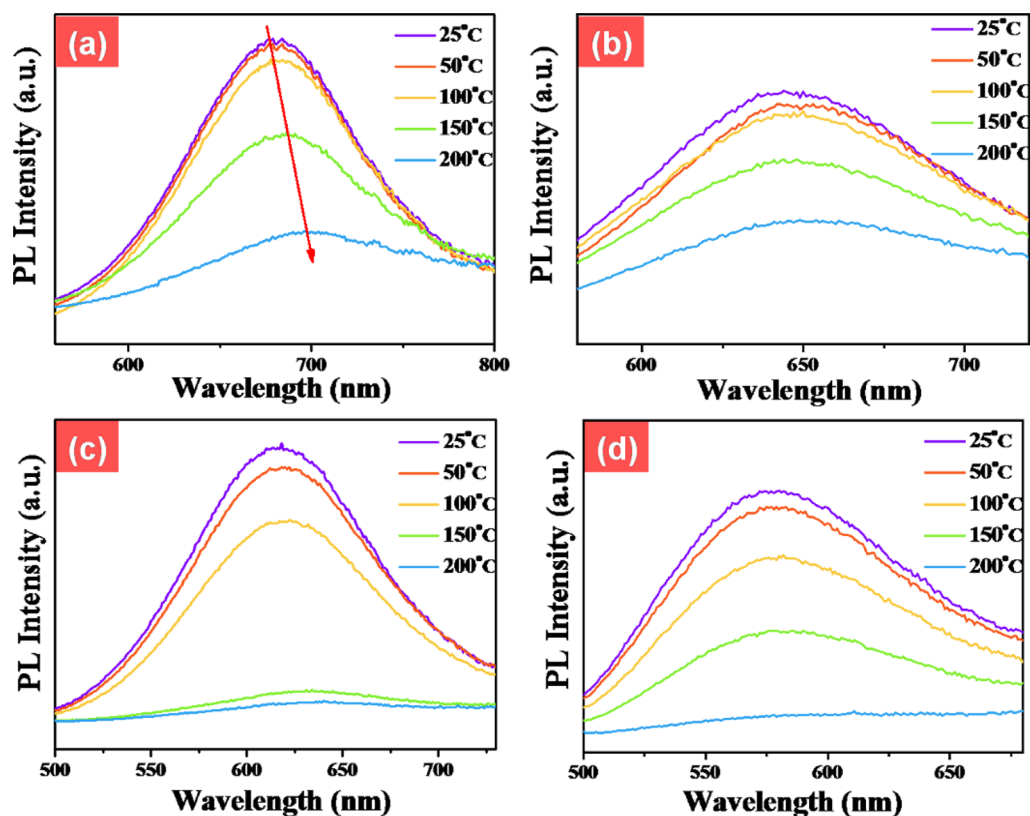
Figure 8. Temperature-dependent PL spectra of CIS/ZnS QDs with Cu/In ratios of (a) 1/1, (b) 1/2, (c)1/4, and (d)1/6 from 25 to 200 °C.
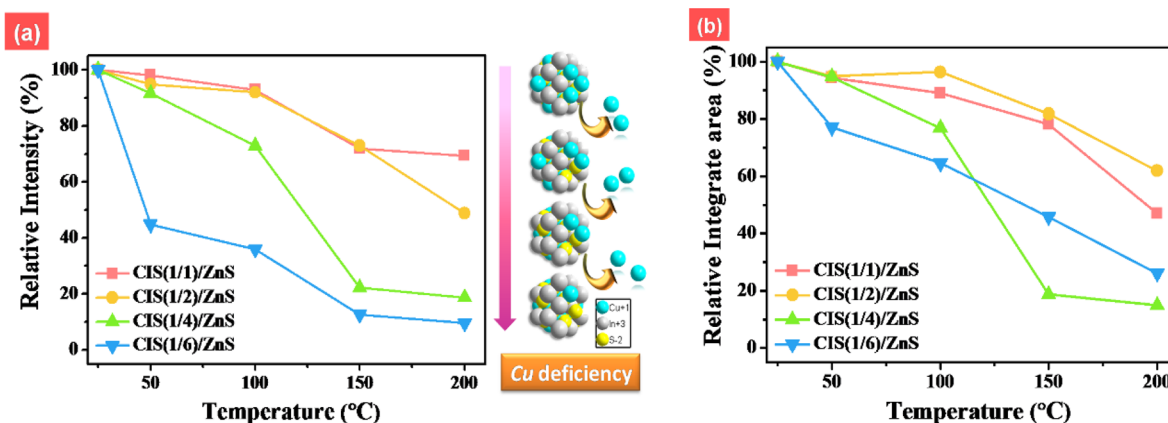

Figure 9. Plot of (a) relative intensity and (b) relative integrate area of CIS/ZnS QDs with [Cu]/[In] ratios of 1/1, 1/2, 1/4, and 1/6 from 25 to 200 °C.

higher than that for [Cu]/[In] = 1/1. We speculate that the high population Cu-deficient QDs may provide the broad spectra. Comparing [Cu]/[In] = 1/4 with [Cu]/[In] = 1/6, the result for [Cu]/[In] = 1/4 was higher than that for [Cu]/[In] = 1/6 before 100 °C. This result may be ascribed to the fact that [Cu]/[In] = 1/4 has optimal DAP recombination, presenting high intensity. However, we can observe that the result for [Cu]/[In] = 1/6 was higher than that for [Cu]/[In] = 1/4 after 100 °C. Similarly, we also speculate that high population Cu-deficient QDs may provide the broad spectra.

3.4. Electroluminescence Performances of the QD-Assisted White LEDs. White LED (WLED) devices convert electrical energy to light much more efficiently than conventional lighting sources. There is growing interest in developing WLEDs for applications in illumination and display. However,

obtaining high-color Ra is difficult because of the lack of the green and red spectral regions. Ziegler et al.[32] fabricated a blue LED with the use of Cd-free silica-coated InP/ZnS QDs with green and yellow phosphors. To fabricate Cd-free QDs with high color rendering index properties, we applied orange ([Cu]/[In] = 1/4) and red ([Cu]/[In] = 1/1) emitting CIS/ZnS QDs, which were blended with a Ba_2SiO_4:Eu^{2+} green phosphor to form WLEDs. According to the TL results, the thermal stability of green-emitting CIS/ZnS QDs ([Cu]/[In] = 1/6) as a thermal stability converter is insufficient. Thermal stability is important in ensuring high efficiency of converter devices.[47,48] Ba_2SiO_4:Eu^{2+} is a commercial green phosphor, which mainly contributes to the PL band from 500 to 550 nm.[49] In an attempt to achieve a wide-ranging spectral region, the other color in the entire visible spectrum was used.
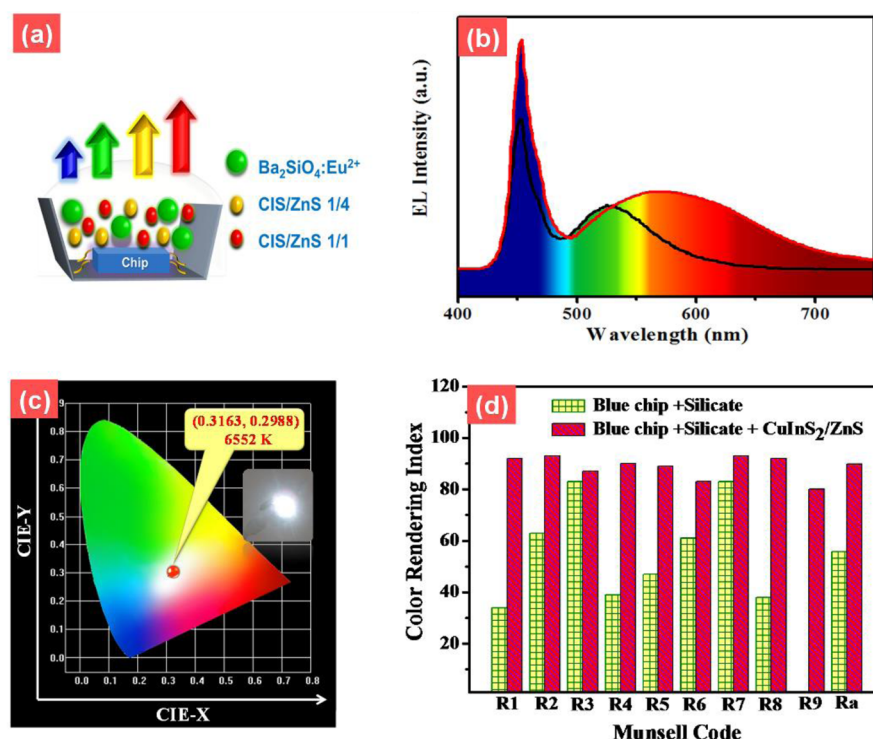
15384

dx.doi.org/10.1021/am503889z | *ACS Appl. Mater. Interfaces* 2014, 6, 15379−15387

Figure 10. (a) Schematic illustration of Ba_2SiO_4:Eu^{2+} phosphor-CIS/ZnS QD-based WLEDs. (b) EL spectra of Ba_2SiO_4:Eu^{2+} phosphor-CIS/ZnS QD-based WLEDs at 20 mA. Schematic illustration of Ba_2SiO_4:Eu^{2+} phosphor-QD-based WLED. (c) CIE diagram of the corresponding QD concentration. Inset is an image of a WLED with CIS/ZnS QDs. (d) CRI of as-fabricated CIS/ZnS QD-assisted Ba_2SiO_4:Eu^{2+} phosphor-based WLEDs and commercial Ba_2SiO_4:Eu^{2+} phosphor-based WLEDs under 20 mA forward bias current.

Therefore, orange- and red-emitting CIS/ZnS QDs and green phosphors Ba_2SiO_4:Eu^{2+} were blended with silicon resins in chloroform. The silicon mixture was laid on InGaN blue LED chips after removing the solvent, as shown in Figure 10a.

Figure 10b shows the electroluminescence (EL) spectra of the fabricated phosphor-QD-based and green phosphor-based WLEDs. The 455 nm band is attributed to the blue chips, and the 500−700 nm emission bands are ascribed to the green phosphors and orange- and red-emitting CIS/ZnS QDs. The luminous efficiency of this device was 32.7 lm/W at 20 mA. Chen et al. fabricated YAG:Ce^{3+} based LEDs with red emissive CIS QDs; their results showed higher efficiency than in our study.[49] The diversity may be ascribed to using different phosphors and LED chip. Figure 10c shows CIE chromaticity color coordinates of 0.3163 and 0.2988 and color temperature (T_c) found at 6552 K, indicating the suitability of the WLEDs. In general, the CRI is a quantitative value, which presents the capability of a light source compared with sunlight. The CRI value is regarded as the Ra, which characterizes the average value of R1−R8. Numbers designate the hues in the Munsell color system.[31] Therefore, compared with the commercial green phosphor-based LEDs, the integrated CIS/ZnS QDs and Ba_2SiO_4:Eu^{2+} phosphor WLED showed a high Ra of 90, as shown in Figure 10d. Consequently, a wide-ranging spectral region was generated. The achieved CRI value of R1 and R8 was enhanced by adding the CIS/ZnS QDs. Moreover, CRI R9 also presented the improved color rendering of a red region from 0 to 82. Orange- and red-emitting CIS/ZnS QDs had broader emission regions to improve CRI values.

4. CONCLUSIONS

Chalcopyrite CIS QDs with various [Cu]/[In] ratios were synthesized through a simple solvothermal method. Color-tunable CIS QDs were successfully synthesized by tuning the [Cu]/[In] molar ratio strategies. The radiative pathway was developed by DAP recombination, resulting in a broad PL band. CIS QD crystal structure was elucidated using bulk model materials in observing the structural and PL emission of the QDs with different [Cu]/[In] molar ratios. CIS core QDs were coated with ZnS shell to obtain highly luminescent CIS/ZnS QDs, and authentic blue shifts were found in the emission relative to the original core CIS QDs. The temperature-dependent PL spectra of the CIS/ZnS QDs showed thermal stability relative to Cu-deficient CIS QDs. The WLEDs were fabricated using green phosphor Ba_2SiO_4:Eu^{2+}, as well as orange- and red-emitting CIS/ZnS QDs. The QD-WLEDs exhibited 36.7 lm/W luminous efficacies at 20 mA forward current and high CRI values of ∼90.

■ AUTHOR INFORMATION

Corresponding Author
*E-mail: rsliu@ntu.edu.tw.

Notes
The authors declare no competing financial interest.

■ REFERENCES

(1) Talapin, D. V.; Lee, J. S.; Kovalenko, M. V.; Shevchenko, E. V. Prospects of Colloidal Nanocrystals for Electronic and Optoelectronic Applications. *Chem. Rev.* **2010**, *110*, 389−458.

(2) Kamat, P. V. Quantum Dot Solar Cells. Semiconductor Nanocrystals as Light Harvesters. *J. Phys. Chem. C* **2008**, *112*, 18737−18753.

(3) Smith, A. M.; Duan, H. W.; Mohs, A. M.; Nie, S. M. Bioconjugated Quantum Dots for In Vivo Molecular and Cellular Imaging. *Adv. Drug Delivery Rev.* **2008**, *60*, 1226−1240.

(4) Scholes, G. D. Controlling the Optical Properties of Inorganic Nanoparticles. *Adv. Funct. Mater.* **2008**, *18*, 1157−1172.

(5) Aboulaich, A.; Michalska, M.; Schneider, R.; Potdevin, A.; Deschamps, J.; Deloncle, R.; Chadeyron, G.; Mahiou, R. Ce-Doped YAG Nanophosphor and Red Emitting $CuInS_2$/ZnS Core/Shell Quantum Dots for Warm White Light-Emitting Diode with High Color Rendering Index. *ACS Appl. Mater. Interfaces* **2014**, *6*, 252−258.

(6) Bharali, D. J.; Lucey, D. W.; Jayakumar, H.; Pudavar, H. E.; Prasad, P. N. Folate-Receptor-Mediated Delivery of InP Quantum Dots for Bioimaging Using Confocal and Two-Photon Microscopy. *J. Am. Chem. Soc.* **2005**, *127*, 11364−11371.

(7) Yong, K.-T.; Ding, H.; Roy, I.; Law, W.-C.; Bergey, E. J.; Maitra, A.; Prasad, P. N. Imaging Pancreatic Cancer Using Bioconjugated InP Quantum Dots. *ACS Nano* **2009**, *3*, 502−510.

(8) Xie, R.; Rutherford, M.; Peng, X. Formation of High-Quality I−III−VI Semiconductor Nanocrystals by Tuning Relative Reactivity of Cationic Precursors. *J. Am. Chem. Soc.* **2009**, *131*, 5691−5697.

(9) Zhong, H. Z.; Zhou, Y.; Ye, M. F.; He, Y. J.; Ye, J. P.; He, C.; Yang, C. H.; Li, Y. F. Controlled Synthesis and Optical Properties of Colloidal Ternary Chalcogenide $CuInS_2$ Nanocrystals. *Chem. Mater.* **2008**, *20*, 6434−6443.

(10) Li, L.; Daou, T. J.; Texier, I.; Tran Thi Kim, C.; Nguyen Quang, L.; Reiss, P. Highly Luminescent $CuInS_2$/ZnS Core/Shell Nanocrystals: Cadmium-Free Quantum Dots for In Vivo Imaging. *Chem. Mater.* **2009**, *21*, 2422−2429.

(11) Li, T. L.; Teng, H. Solution Synthesis of High-Quality $CuInS_2$ Quantum Dots as Sensitizers for TiO_2 Photoelectrodes. *J. Mater. Chem.* **2010**, *20*, 3656−3664.

(12) Nose, K.; Soma, Y.; Omata, T.; Otsuka-Yao-Matsuo, S. Synthesis of Ternary $CuInS_2$ Nanocrystals; Phase Determination by Complex Ligand Species. *Chem. Mater.* **2009**, *21*, 2607−2613.

(13) Nose, K.; Omata, T.; Otsuka-Yao-Matsuo, S. Colloidal Synthesis of Ternary Copper Indium Diselenide Quantum Dots and Their Optical Properties. *J. Phys. Chem. C* **2009**, *113*, 3455−3460.

(14) Allen, P. M.; Bawendi, M. G. Ternary I−III−VI Quantum Dots Luminescent in the Red to Near-Infrared. *J. Am. Chem. Soc.* **2008**, *130*, 9240−9241.

(15) Zhong, H. Z.; Wang, Z. B.; Bovero, E.; Lu, Z. H.; Van Veggel, F. C. J. M.; Scholes, G. D. Colloidal $CuInSe_2$ Nanocrystals in the Quantum Confinement Regime: Synthesis, Optical Properties, and Electroluminescence. *J. Phys. Chem. C* **2011**, *115*, 12396−12402.

(16) Pan, D.; Wang, X.; Zhou, Z. H.; Chen, W.; Xu, C.; Lu, Y. Synthesis of Quaternary Semiconductor Nanocrystals with Tunable Band Gaps. *Chem. Mater.* **2009**, *21*, 2489−2493.

(17) Mao, B. D.; Chuang, C. H.; Wang, J. W.; Burda, C. Synthesis and Photophysical Properties of Ternary I−III−VI $AgInS_2$ Nanocrystals: Intrinsic versus Surface States. *J. Phys. Chem. C* **2011**, *115*, 8945−8954.

(18) Y Hamanaka, Y.; Ogawa, T.; Tsuzuki, M.; Kuzuya, T. Photoluminescence Properties and Its Origin of $AgInS_2$ Quantum Dots with Chalcopyrite Structure. *J. Phys. Chem. C* **2011**, *115*, 1786−1792.

(19) Uematsu, T.; Doi, T.; Torimoto, T.; Kuwabata, S. Preparation of Luminescent $AgInS_2$−$AgGaS_2$ Solid Solution Nanoparticles and Their Optical Properties. *J. Phys. Chem. Lett.* **2010**, *1*, 3283−3287.

(20) Castro, S. L.; Bailey, S. G.; Raffaelle, R. P.; Banger, K. K.; Hepp, A. F. Synthesis and Characterization of Colloidal $CuInS_2$ Nanoparticles from a Molecular Single-Source Precursor. *J. Phys. Chem. B* **2004**, *108*, 12429−12435.

(21) Zhong, H. Z.; Lo, S. S.; Mirkovic, T.; Li, Y. C.; Ding, Y. Q.; Li, Y. F.; Scholes, G. D. Noninjection Gram-Scale Synthesis of Monodisperse Pyramidal $CuInS_2$ Nanocrystals and Their Size-Dependent Properties. *ACS Nano* **2010**, *4*, 5253−5262.

(22) Pons, T.; Pic, E.; Lequeux, N.; Cassette, E.; Bezdetnaya, L.; Guillemin, F.; Marchal, F.; Dubertret, B. Cadmium-Free $CuInS_2$/ZnS Quantum Dots for Sentinel Lymph Node Imaging with Reduced Toxicity. *ACS Nano* **2010**, *4*, 2531−2538.

(23) van Sark, W.; Frederix, P.; Bol, A.; Gerritsen, H.; Meijerink, A. Blueing, Bleaching, and Blinking of Single CdSe/ZnS Quantum Dots. *ChemPhysChem* **2002**, *3*, 871−879.

(24) Hofhuis, J.; Schoonman, J.; Goossens, A. Elucidation of the Excited-State Dynamics in $CuInS_2$ Thin Films. *J. Phys. Chem. C* **2008**, *112*, 15052−15059.

(25) Krustok, J.; Raudoja, J.; Schon, J. H.; Yakushev, M.; Collan, H. The Role of Deep Donor−Deep Acceptor Complexes in CIS-Related Compounds. *Thin Solid Films* **2000**, *361*, 406−410.

(26) Kuo, K.-T.; Chen, S.-Y.; Cheng, B.-M.; Lin, C.-C. Synthesis and Characterization of Highly Luminescent $CuInS_2$ and $CuInS_2$/ZnS (Core/Shell) Nanocrystals. *Thin Solid Films* **2008**, *517*, 1257−1261.

(27) Song, W. S.; Yang, H. Efficient White-Light-Emitting Diodes Fabricated from Highly Fluorescent Copper Indium Sulfide Core/Shell Quantum Dots. *Chem. Mater.* **2012**, *24*, 1961−1967.

(28) Chen, B. K.; Zhong, H. Z.; Zhang, W. Q.; Tan, Z. A.; Li, Y. F.; Yu, C. R.; Zhai, T. Y.; Bando, Y.; Yang, S. Y.; Zou, B. S. Highly Emissive and Color-Tunable $CuInS_2$-Based Colloidal Semiconductor Nanocrystals: Off-Stoichiometry Effects and Improved Electroluminescence Performance. *Adv. Funct. Mater.* **2012**, *22*, 2081−2088.

(29) Nakamura, S.; Fasol, G. Nakamura, S.; Fasol, G. *The Blue Laser Diode: GaN Based Light Emitters and Laser*; Springer: Berlin, 1996.

(30) Nyman, M.; Shea-Rohwer, L. E.; Martin, J. E.; Provencio, P. Nano-YAG:Ce Mechanisms of Growth and Epoxy-Encapsulation. *Chem. Mater.* **2009**, *21*, 1536−1542.

(31) Jang, H. S.; Yang, H.; Kim, S. W.; Han, J. Y.; Lee, S. G.; Jeon, D. Y. White Light-Emitting Diodes with Excellent Color Rendering Based on Organically Capped CdSe Quantum Dots and Sr_3SiO_5:Ce^{3+},Li^+ Phosphors. *Adv. Mater.* **2008**, *20*, 2696−2702.

(32) Ziegler, J.; Xu, S.; Kucur, E.; Meister, F.; Batentschuk, M.; Gindele, F.; Nann, T. Silica-Coated InP/ZnS Nanocrystals as Converter Material in White LEDs. *Adv. Mater.* **2008**, *20*, 4068−4073.

(33) Murray, C. B.; Norris, D. J.; Bawendi, M. G. Synthesis and Characterization of Nearly Monodisperse CdE (E = Sulfur, Selenium, Tellurium) Semiconductor Nanocrystallites. *J. Am. Chem. Soc.* **1993**, *115*, 8706−8715.

(34) Nakamura, H.; Kato, W.; Uehara, M.; Nose, K.; Omata, T.; Otsuka-Yao-Matsuo, S.; Miyazaki, M.; Maeda, H. Tunable Photoluminescence Wavelength of Chalcopyrite $CuInS_2$-Based Semiconductor Nanocrystals Synthesized in a Colloidal System. *Chem. Mater.* **2006**, *18*, 3330−3335.

(35) Hamanaka, Y.; Ogawa, T.; Tsuzuki, M.; Kuzuya, T. Photoluminescence Properties and Its Origin of $AgInS_2$ Quantum Dots with Chalcopyrite Structure. *J. Phys. Chem. C* **2011**, *115*, 1786−1792.

(36) Uehara, M.; Watanabe, K.; Tajiri, Y.; Nakamura, H.; Maeda, H. Synthesis of $CuInS_2$ Fluorescent Nanocrystals and Enhancement of Fluorescence by Controlling Crystal Defect. *J. Chem. Phys.* **2008**, *129*, 134709-1−134709-6.

(37) Kim, Y.-K.; Ahn, S.-H.; Chung, K.; Cho, Y.-S.; Choi, C.-J. The Photoluminescence of $CuInS_2$ Nanocrystals: Effect of Non-stoichiometry and Surface Modification. *J. Mater. Chem.* **2012**, *22*, 1516−1520.

(38) Dai, M. L.; Ogawa, S.; Kameyama, T.; Okazaki, K.; Kudo, A.; Kuwabata, S.; Tsuboi, Y.; Torimoto, T. Tunable Photoluminescence from the Visible to Near-infrared Wavelength Region of Non-stoichiometric $AgInS_2$ Nanoparticles. *J. Mater. Chem.* **2012**, *22*, 12851−12858.

(39) Nam, D. E.; Song, W. S.; Yang, H. Noninjection, One-Pot Synthesis of Cu-Deficient $CuInS_2$/ZnS Core/Shell Quantum Dots and Their Fluorescent Properties. *J. Colloid Interface Sci.* **2011**, *361*, 491−496.

15386

dx.doi.org/10.1021/am503889z | *ACS Appl. Mater. Interfaces* 2014, 6, 15379−15387

(40) Omata, T.; Nose, K.; Otsuka-Yao-Matsuo, S. Size Dependent Optical Band Gap of Ternary I−III−VI$_2$ Semiconductor Nanocrystals. *J. Appl. Phys.* **2009**, *105*, 073106-1−073106-5.

(41) Jaffe, J. E.; Zunger, A. Electronic Structure of The Ternary Chalcopyrite Semiconductors CuAlS$_2$, CuGaS$_2$, CuInS$_2$, CuAlSe$_2$, CuGaSe$_2$, and CuInSe$_2$. *Phys. Rev. B* **1983**, *28*, 5822−5847.

(42) Chen, Y.; Li, S.; Huang, L.; Pan, D. Green and Facile Synthesis of Water-Soluble Cu−In−S/ZnS Core/Shell Quantum Dots. *Inorg. Chem.* **2013**, *52*, 7819−7821.

(43) Pan, D.; An, L.; Sun, Z.; Hou, W.; Yang, Y.; Yang, Z.; Lu, Y. Synthesis of Cu−In−S Ternary Nanocrystals with Tunable Structure and Composition. *J. Am. Chem. Soc.* **2008**, *130*, 5620−5621.

(44) Yoshino, K.; Ikari, T.; Shirakata, S.; Miyake, H.; Hiramatsu, K. Sharp Band Edge Photoluminescence of High-Purity CuInS$_2$ Single Crystals. *Appl. Phys. Lett.* **2001**, *78*, 742−744.

(45) Yakushev, M. V.; Mudryi, A. V.; Victorov, I. V.; Krustok, J.; Mellikov, E. Energy of Excitons in CuInS$_2$ Single Crystals. *Appl. Phys. Lett.* **2006**, *88*, 011922−1−3.

(46) Jing, P.; Zheng, J.; Ikezawa, M.; Liu, X.; Lv, S.; Kong, X.; Zhao, J.; Masumoto, Y. Temperature-Dependent Photoluminescence of CdSe-Core CdS/CdZnS/ZnS-Multishell Quantum Dots. *J. Phys. Chem. C* **2009**, *113*, 13545−13550.

(47) Woo, J. Y.; Kim, K. N.; Jeong, S.; Han, C.-S. Thermal Behavior of a Quantum Dot Nanocomposite as A Color Converting Material and Its Application to White LED. *Nanotechnology* **2010**, *21*, 495704-1−495704-8.

(48) Wang, M.; Zhang, X.; Hao, Z.; Ren, X.; Luo, Y.; Zhao, H.; Wang, X.; Zhang, J. Long-Lasting Phosphorescence in BaSi$_2$O$_2$N$_2$:Eu^{2+} and Ba$_2$SiO$_4$:Eu^{2+} Phases for X-Ray and Cathode Ray Tubes. *J. Electrochem. Soc.* **2010**, *157*, H178−H181.

(49) Chen, B. K.; Zhou, Q. C.; Li, J. F.; Zhang, F.; Liu, R. B.; Zou, B. S. Red Emissive CuInS$_2$ Based Nanocrystals: A Potential Phosphor for Warm White Light-Emitting Diodes. *Opt. Express* **2013**, *21*, 10105.